



**HAL**  
open science

## Sensitivity of montane grassland water fluxes to warming and elevated CO<sub>2</sub> from local to catchment scale: A case study from the Austrian Alps

Matevž Vremec, Peter Burek, Luca Guillaumot, Jesse Radolinski, Veronika Forstner, Markus Herndl, Christine Stumpp, Michael Bahn, Steffen Birk

### ► To cite this version:

Matevž Vremec, Peter Burek, Luca Guillaumot, Jesse Radolinski, Veronika Forstner, et al.. Sensitivity of montane grassland water fluxes to warming and elevated CO<sub>2</sub> from local to catchment scale: A case study from the Austrian Alps. *Journal of Hydrology: Regional Studies*, 2024, 56, pp.101970. 10.1016/j.ejrh.2024.101970 . hal-04717113

HAL Id: hal-04717113

<https://brgm.hal.science/hal-04717113v1>

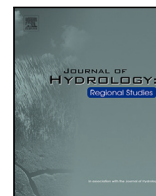
Submitted on 1 Oct 2024

**HAL** is a multi-disciplinary open access archive for the deposit and dissemination of scientific research documents, whether they are published or not. The documents may come from teaching and research institutions in France or abroad, or from public or private research centers.

L'archive ouverte pluridisciplinaire **HAL**, est destinée au dépôt et à la diffusion de documents scientifiques de niveau recherche, publiés ou non, émanant des établissements d'enseignement et de recherche français ou étrangers, des laboratoires publics ou privés.



Distributed under a Creative Commons Attribution 4.0 International License



## Sensitivity of montane grassland water fluxes to warming and elevated CO<sub>2</sub> from local to catchment scale: A case study from the Austrian Alps

Matevž Vremec<sup>a,\*</sup>, Peter Burek<sup>b</sup>, Luca Guillaumot<sup>b,c</sup>, Jesse Radolinski<sup>d,e</sup>, Veronika Forstner<sup>a,f</sup>, Markus Herndl<sup>f</sup>, Christine Stumpp<sup>g</sup>, Michael Bahn<sup>d</sup>, Steffen Birk<sup>a</sup>

<sup>a</sup> Department of Earth Sciences, NAWI Graz Geocenter, University of Graz, 8010 Graz, Austria

<sup>b</sup> International Institute for Applied Systems Analysis, Laxenburg, Austria

<sup>c</sup> Water, Environment, Processes and Analyses Division, BRGM-French Geological Survey, Orleans, France

<sup>d</sup> Department of Ecology, University of Innsbruck, Innsbruck, Austria

<sup>e</sup> Department of Environmental Science and Technology, University of Maryland, College Park, MD, USA

<sup>f</sup> Institute of Plant Production and Cultural Landscape, Agricultural Research and Education Centre, Irnding-Donnersbachtal, Austria

<sup>g</sup> University of Natural Resources and Life Sciences, Vienna, Department of Water, Atmosphere and Environment, Institute of Soil Physics and Rural Water Management, Muthgasse 18, 1190 Vienna, Austria

### ARTICLE INFO

#### Keywords:

Hydrologic response  
Hydrological models  
Climate change  
Montane grassland  
Lysimeter

### ABSTRACT

Study region: Montane grassland within the Gulling catchment, Austrian Alps. Study focus: A climate-change experiment in a grassland ecosystem used lysimeters and HYDRUS-1D models to quantify changes in evapotranspiration (ET) and groundwater recharge (GWR) due to warming (+3 °C) and elevated CO<sub>2</sub> concentrations (ΔCO<sub>2</sub>; +300 ppm). Findings at the plot-scale were generalized and transferred to the surrounding catchment, half comprised of grassland, using three lumped rainfall–runoff models and two spatially-distributed Community Water Models, differing in soil hydraulic properties.

New hydrological insights for the region: Warming increased ET and decreased GWR and river discharge compared to ambient conditions. ΔCO<sub>2</sub> increased stomatal resistance, which partially offset warming effects. In scenarios combining warming and ΔCO<sub>2</sub>, the impact of warming was higher than ΔCO<sub>2</sub> effect. Elevation influenced the sensitivity of ET to warming, which was greater at the catchment scale than at the plot scale, while GWR was more sensitive to warming at the plot scale. Under dry conditions, GWR and discharge exhibited increased sensitivity to warming at both scales. HYDRUS-1D successfully reproduced lysimeter experiment results and their sensitivity to warming and ΔCO<sub>2</sub>. Despite model agreement on water flux sensitivity to climate changes, the varying response magnitudes highlight the need for a multi-model approach in climate impact assessments. This study provides insights into how climate change might impact hydrological dynamics of montane grassland systems across the Central European Alps.

\* Corresponding author.

E-mail address: [matevz.vremec@uni-graz.at](mailto:matevz.vremec@uni-graz.at) (M. Vremec).

<https://doi.org/10.1016/j.ejrh.2024.101970>

Received 27 June 2024; Received in revised form 3 September 2024; Accepted 5 September 2024

Available online 13 September 2024

2214-5818/© 2024 The Author(s). Published by Elsevier B.V. This is an open access article under the CC BY license (<http://creativecommons.org/licenses/by/4.0/>).

## 1. Introduction

Climate change is disrupting the hydrological cycle not only by altering precipitation patterns but also by increasing evaporative demand (IPCC, 2021; Allan et al., 2020; Teuling, 2018; Duethmann and Blöschl, 2018). Such changes may ultimately lead to reductions in both surface water and groundwater resources in various regions (Green et al., 2011; Haslinger et al., 2022). Further, recent work by Zhang et al. (2023) suggests that the sensitivity of river discharge to changes in evapotranspiration (ET) due to warming is greater than previously thought. Thus, understanding the impact of changing ET on water fluxes in a changing climate is critical for future assessments of water resources.

Rainfall–runoff models are commonly used to investigate how changes in precipitation and ET due to warming (denoted as  $\Delta T$ ) and elevated  $\text{CO}_2$  concentrations (denoted as  $\Delta \text{CO}_2$ ) impact water fluxes at plot, regional, and global scale (Duethmann et al., 2020; Karlsson et al., 2016; Bastola et al., 2011; Broderick et al., 2016). Global-scale studies (Milly and Dunne, 2016; Berg et al., 2016; Zhang et al., 2023) have shown that the rise in terrestrial ET attributed to global warming often surpasses precipitation increases, resulting in continental drying. This phenomenon is largely driven by the direct effects of warming, which increase the vapor pressure deficit and the Clausius-Clapeyron slope, thereby increasing potential evapotranspiration (PET) (Scheff and Frierson, 2014; Milly and Dunne, 2016). In arid climates, the greening effect due to  $\Delta \text{CO}_2$  can further amplify the effects of  $\Delta T$ , leading to higher water use for vegetation (Ukkola et al., 2016). Conversely, in humid regions with dense vegetation,  $\Delta \text{CO}_2$  can mitigate  $\Delta T$  effects and contribute to water conservation through partial stomatal closure, a process by which plants close the openings on their leaves to regulate water loss (Leakey et al., 2009; Milly and Dunne, 2016; Ukkola et al., 2016; Yang et al., 2021). The contrasting or intensifying impacts of  $\Delta T$  and  $\Delta \text{CO}_2$  on water fluxes are largely due to variations in regional climate and vegetation responses, highlighting the need for region-specific assessments of climate change impacts (Faticchi et al., 2016).

Prior research conducted in the Alpine region has predominantly focused on exploring the effects of climate change on water fluxes by analyzing historical river discharge observations (Duethmann and Blöschl, 2018; Duethmann et al., 2020) or employing hydrological models combined with regional climate change scenarios (Wagner et al., 2017; Hanus et al., 2021). These studies commonly report that warming leads to a decrease in overall river discharge and an increase in ET, especially in summer. However, these findings were mainly derived from individual modeling exercises and offer limited insight into the sensitivity of specific water fluxes at different scales or across different models. Several studies have demonstrated that the choice of the hydrological model can affect the simulated response of groundwater recharge and river discharge to climate change (Moeck et al., 2016; Karlsson et al., 2016; Broderick et al., 2016). This underscores the importance of empirical data to support these results and the importance of a multi-model approach to better constrain the impact of  $\Delta T$  and  $\Delta \text{CO}_2$  on water fluxes (Faticchi et al., 2016).

To address this knowledge gap, a long-term climate-change experiment was conducted in a montane grassland in the Austrian Alps (Piepho et al., 2017; Herndl et al., 2011), a region where grassland ecosystems cover about 40%–45% of the land area and play a central role in regulating the water balance (BMLRT, 2020; Inauen et al., 2013; Wieser et al., 2008). Data from this experiment, analyzed by Forstner et al. (2021) for the period 2015–2018, was derived from six high-precision weighing lysimeters operated under conditions of increased temperature and elevated  $\text{CO}_2$  concentrations. The study found that warming (+3 °C) led to an increase in ET and a decrease in groundwater recharge, while  $\Delta \text{CO}_2$  (+300 ppm) had the opposite effect, leading to a decrease in ET and increase in groundwater recharge. These effects are attributed to the reduction in plant transpiration due to partial stomatal closure from  $\text{CO}_2$  enrichment (Vremec et al., 2023; Leakey et al., 2009). However, when both  $\Delta T$  and  $\Delta \text{CO}_2$  were present, the  $\Delta \text{CO}_2$  effect did not fully counterbalance the increased ET caused by  $\Delta T$ , resulting in a net increase in ET compared to current ambient climatic conditions.

In this study, we expand our understanding of how climate change affects the hydrological cycle, by moving beyond plot-scale investigations of montane grasslands water fluxes (lysimeter experiments and HYDRUS-1D models) to a catchment scale analysis utilizing five rainfall–runoff models. This includes three lumped-parameter models (GR4J, HyMod, and HBV<sub>EDU</sub>) and two spatially-distributed Community Water Model (CWatM) models. Specifically, we evaluate

- how changes in PET, driven by  $\Delta T$  and  $\Delta \text{CO}_2$ , impact the water fluxes observed at plot scale and to which extent these observations can be reproduced by soil hydrological modeling;
- how and why the impacts of changes in PET on modeled water fluxes differ from the plot scale to the catchment scale;
- how the simulated impacts at catchment scale vary across different rainfall–runoff models.

This multi-model approach is aimed to underscore the broader implications and to address the uncertainties associated with upscaling the climate-driven changes of water fluxes through various models.

## 2. Data and methods

### 2.1. Study site

The investigated area was the Gulling catchment, located in the Enns valley of Austria, adjacent to the experimental facility shown in Fig. 1. The catchment spans an area of 156 km<sup>2</sup> and covers an altitude range from 644 to 2220 m, with a mean elevation of 1430 m. Half of the catchment comprises grassland (51%; mainly including pastures, alpine meadows, and extensive and managed grassland), 48% is forested, while the remaining 1% consists of high elevation bare rock surfaces and water bodies. The soil in the catchment is mainly composed of cambisol (62%), podzol (35%), and luvisol (3%). The catchment receives an average annual

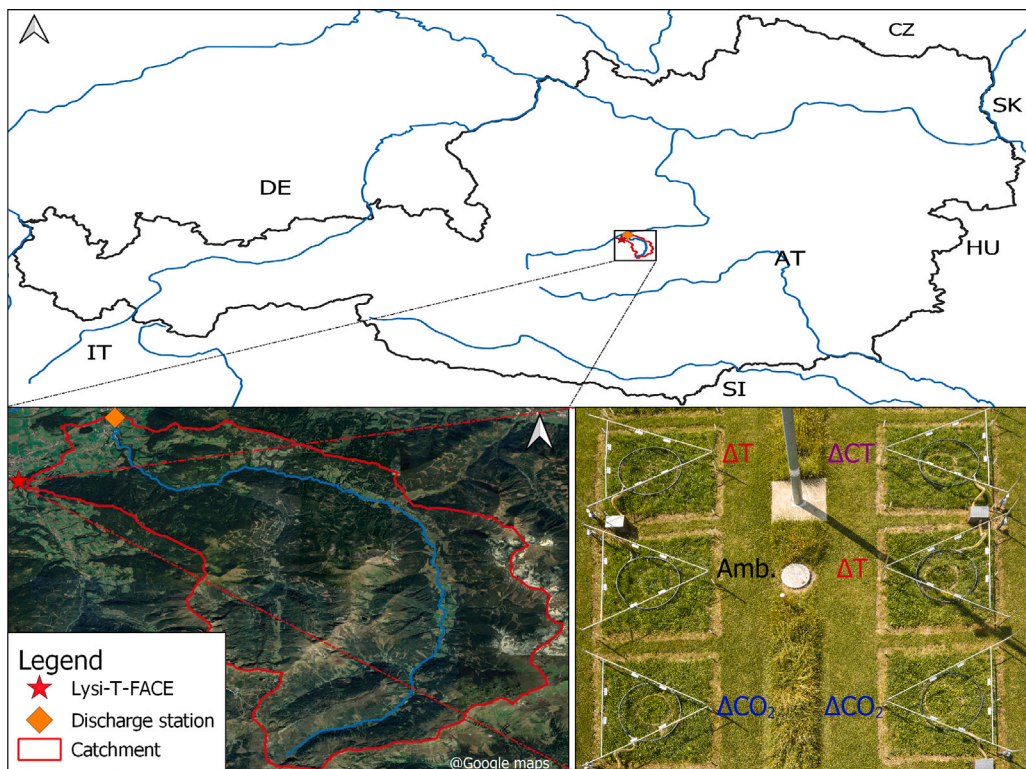


Fig. 1. Location of the Gullung catchment and the Lysi-T-FACE experimental site with their different factor combinations: ambient (Amb.), +3 °C ( $\Delta T$ ), +300 ppm  $\text{CO}_2$  ( $\Delta \text{CO}_2$ ), and +3 °C combined with +300 ppm  $\text{CO}_2$  ( $\Delta \text{CT}$ ).

precipitation of 1450 mm (1990–2016), is influenced by snowmelt during spring, and has an average annual temperature of 5.2 °C (1990–2016).

The main experimental plot site was the Lysi-T-FACE experiment conducted at the AREC Raumberg-Gumpenstein research station (Piepho et al., 2017; Herndl et al., 2011). The objective of this climate-change experiment was to investigate the effects of  $\Delta T$ ,  $\Delta \text{CO}_2$ , and drought on the ecohydrology of managed montane grassland. The facility is situated at an elevation of 707 m above sea level, close to the confluence of the Enns and Donnersbach rivers in the eastern Austrian Alps. Among the plant communities present are grasses such as *Arrhenatherum elatius* and *Festuca pratensis*, and legumes such as *Lotus corniculatus* and *Trifolium pratense*, which are typical of permanent grassland in the Alps (Schaumberger, 2011). Preliminary analysis revealed three soil horizons at the site ( $A_{ph}$ : 0–25 cm,  $B_v$ : 26–90 cm,  $C_v$ : > 100 cm), with the soil type classified as a Cambisol, primarily consisting of loamy sand with soil texture analyzed according to ÖNORM L 1050 for the A ( $45 \pm 5\%$  sand,  $45 \pm 5\%$  silt, and  $9 \pm 3\%$  clay) and B horizon ( $53 \pm 10\%$  sand,  $37 \pm 8\%$  silt, and  $10 \pm 3\%$  clay). The median bulk density of the upper two horizons is  $1.4 \text{ g cm}^{-3}$ , and the median saturated hydraulic conductivity is 114 cm day (range: 50.5–234.1 cm day $^{-1}$ ). The average annual precipitation at the site is 1077 mm (1991–2020) with an annual mean temperature of 8.5 °C (1991–2020).

## 2.2. Workflow

Our approach to assess the individual and combined effects of  $\Delta T$  and  $\Delta \text{CO}_2$  on the sensitivity of potential evapotranspiration (PET), and in turn on actual evapotranspiration, groundwater recharge, and river discharge at both the plot and catchment scales, consisted of three main steps (Fig. 2):

1. Quantification of the effects of  $\Delta T$  and  $\Delta \text{CO}_2$  at the plot scale using lysimeter soil water fluxes.
2. Generalization of plot-scale findings to compute PET for different levels of  $\Delta T$  and  $\Delta \text{CO}_2$ , cross-checking the results with lysimeter data.
3. Simulation of three climate change scenarios at the plot and catchment level, mirroring the lysimeter experiment, to compare water flux changes against current ambient climatic conditions.

Each step followed a *storyline* approach (Shepherd, 2019; Buitink et al., 2021), where the current or past hydrological system was influenced by future conditions ( $\Delta T$  and  $\Delta \text{CO}_2$ ). Such approaches have been used to better understand (a) process changes and (b) system response to changes in climate conditions (Van Tiel et al., 2023). We explain each step in more detail below. The first two

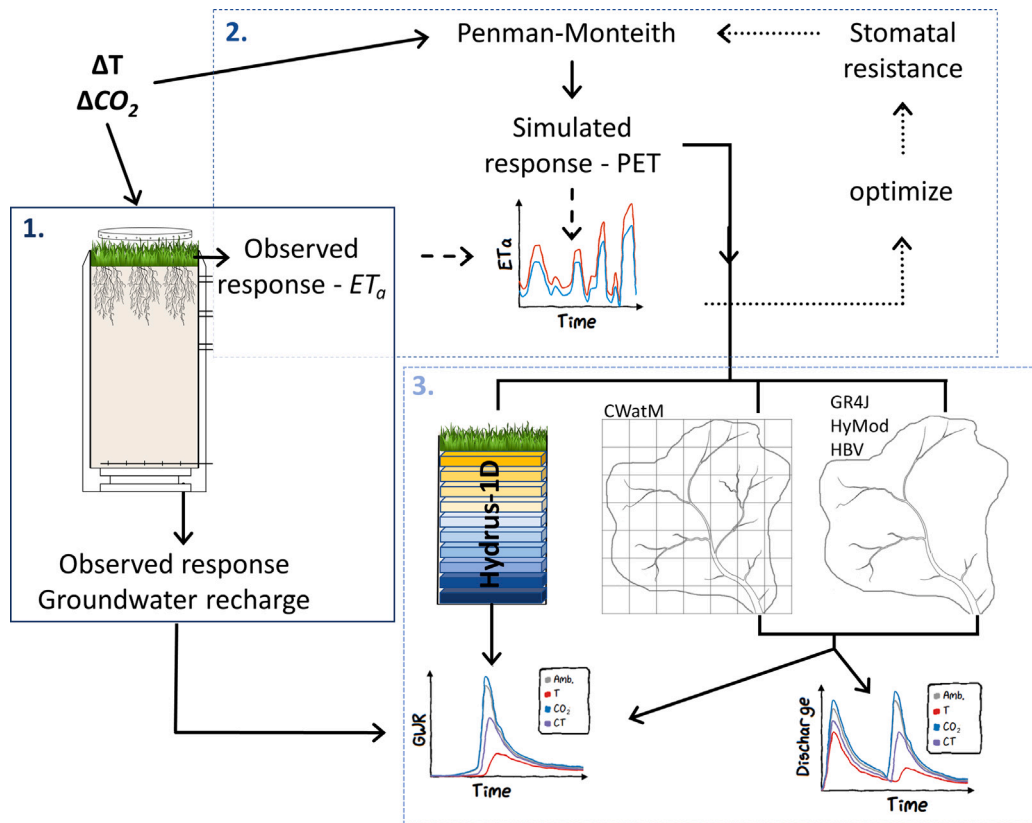


Fig. 2. Schematic representation of the study's workflow, which involved: (1) quantifying responses of lysimeter soil water fluxes to warming ( $\Delta T$ ) and elevated  $CO_2$  concentrations ( $\Delta CO_2$ ); (2) generalizing the findings from lysimeter experiments; and (3) upscaling these results to the catchment level.

steps covered the lysimeter observation period from 2016 to 2021, while the last step covered the years 1990 to 2016 to account for local climate variability and enable comparisons at both plot and catchment levels.

### 2.3. Lysimeter soil water fluxes

In the study, lysimeters were used to quantify the components of the soil water balance, comprising precipitation ( $P$ ), actual evapotranspiration ( $ET_a$ ), groundwater recharge ( $GWR$ ) and the change in the soil water storage  $\Delta S$ , assuming no overland flow occurred:

$$\Delta S = P - ET_a - GWR \quad (1)$$

Data from six high-precision weighing lysimeters, which are part of the Lysi-T-FACE concept that applies a heating treatment and free-air controlled enrichment with  $CO_2$  to open-field plant canopies (Herndl et al., 2011), were used to quantify and generalize the effects of  $\Delta T$  and  $\Delta CO_2$ . Here, the dataset from Forstner et al. (2021) formed the basis for our analysis, which we then extended by expanding the observation period for three more years. The six lysimeters were divided into different treatments: two were treated with  $\Delta CO_2$ , two with  $\Delta T$ , one with both  $\Delta CO_2$  and  $\Delta T$ , and one remained under ambient conditions. To achieve a controlled increase of +300 ppm in  $CO_2$  compared to ambient conditions, the  $\Delta CO_2$ -treated lysimeters were subjected to a Free Air Carbon dioxide Enrichment (FACE) system as described by Miglietta et al. (2001). Temperature control was accomplished using an infrared heater-based free air enrichment system (T-FACE) to raise the temperature by +3 °C (relative to ambient surface temperature), following the method outlined by Kimball (2005). Daily soil water fluxes were calculated by resampling 10-min water balance data to daily sums. Leaf area index (LAI) measurements were conducted throughout the growing season using the AccuPAR LP-80 Ceptometer, with at least 10 measurements per year per lysimeter. A more detailed description of the lysimeter setup can be found in Herndl et al. (2011) and Forstner et al. (2021), as well as in the Supplementary material. We quantified changes in annual lysimeter soil water fluxes for the growing season from 2016 to 2021, a period which included the relatively dry years of 2018 and 2019. The start and end of each growing season were defined based on the thermal approach of Ernst and Loeper (1976), computed using daily average ambient temperature (see Supplementary material). To evaluate the significant effects of  $\Delta T$  and  $\Delta CO_2$  on daily actual evapotranspiration, groundwater recharge, and LAI measurements from the lysimeters, we employed an analysis of variance

(ANOVA) followed by a post hoc Tukey test. We limited our daily  $ET_a$  analysis to days when the  $CO_2$  concentration in  $CO_2$ -enriched lysimeters was within 30% of the target (+300 ppm) and the  $\Delta T$  lysimeters were within 30% of the target temperature increase (+3 °C) ( $0.7 < TAR < 1.3$ ;  $TAR = \text{target achievement ratio}$ ).

#### 2.4. Potential evapotranspiration under $\Delta T$ and $\Delta CO_2$

Potential evapotranspiration for the lysimeter treatments, the plot and catchment scale hydrological models, was computed using the Penman–Monteith (PM) equation (Allen et al., 1998):

$$PET = \frac{1}{\lambda} \left[ \frac{\Delta(R_n - G) + \rho_a c_p k (e_s - e_a) / r_a}{\Delta + \gamma (1 + \frac{r_s}{r_a})} \right] \quad (2)$$

where PET is the potential evapotranspiration [ $kg\ m^{-2}\ d^{-1}$  equivalent to  $mm\ d^{-1}$ ],  $\lambda$  is the latent heat of vaporization [ $MJ\ kg^{-1}$ ],  $\Delta$  is the slope of the saturation vapor pressure curve [ $kPa\ K^{-1}$ ],  $R_n$  [ $MJ\ m^{-2}\ d^{-1}$ ] is the net radiation,  $G$  is the soil heat flux [ $MJ\ m^{-2}\ d^{-1}$ ],  $\rho_a$  is the air density [ $kg\ m^{-3}$ ],  $c_p$  is the specific heat of dry air [ $MJ\ kg^{-1}\ K^{-1}$ ],  $e_s$  is the saturation and  $e_a$  is the actual vapor pressure of the air [ $kPa$ ],  $\gamma$  is the psychrometric constant [ $kPa\ K^{-1}$ ],  $r_s$  is the bulk surface resistance [ $s\ m^{-1}$ ],  $r_a$  is the bulk aerodynamic resistance [ $s\ m^{-1}$ ], and  $k$  is for unit conversion ( $=86\ 400$ ) [ $s\ d^{-1}$ ]. The value of  $r_a$  was calculated using crop height (equation 4 in Allen et al., 1998), with an assumed value of 0.12 LAI following Vremec et al. (2021). Net radiation was computed as incoming net shortwave radiation minus outgoing net longwave radiation, according to equation 40 in Allen et al. (1998). This calculation used measured solar radiation and daily mean, maximum, and minimum temperatures.  $G$  was set to 0 as suggested by Allen et al. (1998).

The PM equation was combined with an adapted  $CO_2$ -dependent stomatal resistance model to capture the effect of  $\Delta CO_2$  on stomatal resistance and LAI (Yang et al., 2019; Vremec et al., 2023, 2024):

$$r_s = \frac{r_l(CO_2)}{LAI} = \frac{r_{r_l-300} \times \left\{ 1 + S_{r_l-CO_2} \times ([CO_2] - 300) \right\}}{LAI} \quad (3)$$

where  $S_{r_l-[CO_2]}$  [ $ppm^{-1}$ ] is the relative sensitivity of  $r_l$  to  $\Delta[CO_2]$ ; and  $r_{r_l-300}$  [ $s\ m^{-1}$ ] is the reference stomatal resistance when atmospheric  $[CO_2]$  is 300 ppm. The relative sensitivity of  $r_l$  to  $\Delta[CO_2]$  represents the change in  $r_l$  per ppm increase in  $[CO_2]$ .

We used the two equations above to (i) assess changes in stomatal resistance under  $\Delta CO_2$  by inversely estimating stomatal resistance at lysimeters with ambient  $CO_2$  and lysimeters treated under  $\Delta CO_2$ , and (ii) obtain  $r_{r_l-300}$  and  $S_{r_l-CO_2}$ , which are necessary to compute PET at any  $CO_2$  concentration. Here,  $r_{r_l-300}$  and  $S_{r_l-CO_2}$  were estimated by comparing calculated PET (using the PM equation) with the measurements obtained from lysimeters. To estimate these parameters, the trust-region reflective least squares algorithm, as implemented in Scipy (Virtanen et al., 2020), was employed. This analysis was conducted only on days when the  $ET_a$  measured by the lysimeter was considered equivalent to the PET demand. The relevant periods were identified according to Vremec et al. (2023), selecting days when plant transpiration was not limited by water availability and the LAI was greater than 2. The periods when water availability affected plant transpiration were defined as days when the soil moisture anomaly index (calculated from the soil water content at a depth of 30 cm) was below  $-2$ . This procedure was performed for all six lysimeters, where approximately 50% of the data was preserved.

Experimental warming of grassland can impact the vapor pressure deficit (VPD) between the inside of the leaves and the outside air, under conditions of (i) constant relative humidity ( $RH = \text{constant}$ ) or (ii) constant actual vapor pressure ( $e_a = \text{constant}$ ) (Kimball, 2005; Scheff and Frierson, 2014):

$$VPD = e_s(1 - RH) = e_s - e_a, \quad (4)$$

where  $RH$  is the near-surface relative humidity. In scenarios where  $e_a$  is constant,  $RH$  would have to decrease. Scheff and Frierson (2014) recommend examining the impact of global warming on PET under constant  $RH$  to observe how variations in  $e_s$  influence VPD and PET. However, to better represent the open-field conditions of our infrared-heated plot, where warming was not performed everywhere (i.e. by global warming), we adapted our model to evaluate the effects on PET under constant  $e_a$  conditions, following Kimball (2005). Recent insights from land surface observations (Douville and Willett, 2023) suggest that such scenarios may indeed reflect real-world conditions over land to some extent, where relative humidity is expected to decrease (Allan et al., 2020). As such, PET was estimated using the Penman–Monteith equation, adjusting the ambient daily temperature by the  $\Delta T$  factor for computing  $e_s$ ,  $\Delta$ , and  $\rho_a$ , thereby increasing VPD and the Clausius-Clapeyron slope, while keeping other variables constant ( $R_n$ ,  $e_a$ ,  $r_a$ ,  $r_s$ ,  $\gamma$ ,  $\lambda$ ,  $c_p$ ). This approach was also applied at the catchment to enable a direct comparison between the different scales. The effects of  $\Delta T$  on PET under constant  $RH$  are also presented in Supplementary material, Figure S8.

The daily meteorological data used to estimate PET were obtained from on-site meteorological, including temperature, wind speed, relative humidity, and solar radiation. LAI data from 2016 to 2021 were derived from AccuPar measurements, while a mean LAI of 2.2, representing the growing season average, was applied to the period from 1990 to 2016. Model performance was analyzed using the Kling-Gupta efficiency (KGE), and the bias was calculated as the mean of the differences between observed and simulated values.

## 2.5. Plot-scale hydrological model

Soil water fluxes at the plot scale were modeled with a HYDRUS-1D model (Šimůnek et al., 2008). This model takes PET as input, and divides it into potential soil evaporation and potential transpiration using Beer's law (Ritchie, 1972). The model then calculates actual transpiration and groundwater recharge based on the availability of water in the root zone, as described by Van Genuchten (1980). The soil water retention and hydraulic conductivity function were characterized using the unimodal Van Genuchten–Mualem model (Van Genuchten, 1980). The soil horizon was divided into three layers, each layer represented by a set of soil hydraulic properties. The meteorological data used for estimating PET, along with the daily precipitation data that served as input for the HYDRUS-1D model, were acquired from the onsite Irnding station (approximately 150 m from the study site), operated by the national meteorological service GeoSphere Austria. PET was estimated according to Section 2.4.

The calibration of the HYDRUS-1D model was performed using daily seepage rates at the lower lysimeter boundary, soil water content, and matric potential data obtained from the ambient weighing lysimeter at a depth of 10 and 30 cm. Given that soil water content rarely reached very dry conditions near the wilting point, we complemented our calibration data with matric potential and soil water content data collected in the drier range (see Supplementary material, Figure S1). This additional dataset was obtained with the WP4C dew point potentiometer from disturbed soil samples. We incorporated this additional dataset to improve the predictive capability, particularly under drier conditions. To capture the effects of both wet and dry years, the entire available period (2016–2021) was used for calibration (Shen et al., 2022). During this period, annual precipitation ranged from 946 mm in 2021 to 1275 mm in 2017, and average annual temperatures varied from 7.9 °C in 2021 to 9.1 °C in 2018.

The DREAM<sub>ZS</sub> (DiffeREntial Evolution Adaptive Metropolis) global optimization algorithm, as implemented in the Spotpy package (Houska et al., 2015) and described by Vrugt (2016), was employed to calibrate the HYDRUS-1D model. With a range of different measurement types for the HYDRUS-1D model, the data likelihood was aggregated as the sum of the logarithmic likelihoods of each measurement type following Schübl et al. (2022). We constrained the uniform prior distributions using physically plausible values derived from previous modeling studies at the site (Stump et al., 2012; Schübl et al., 2022) and laboratory soil analyses, while the standard deviations of the measurement errors were determined using data from the duplicated lysimeters. For more details on the calibration procedure, see Supplementary material.

We undertook the plot-scale modeling exercise for two key reasons. The first was to compare the observed sensitivity of water fluxes, based on lysimeter data, to those predicted by our simulations at the plot scale (2016–2021). The second was to obtain plot-scale water flux data for the period 1990–2016, enabling a comparison of water fluxes at plot and catchment scale within the same timeframe.

### 2.5.1. Catchment rainfall–runoff models

In this catchment modeling study, we selected a range of widely applied hydrological models, each with varying complexity and distinct methodologies for representing soil and water routing processes. The spatially-distributed Community Water Model (CWatM) model was chosen for its physically-based representation of hydrological processes, including infiltration, evapotranspiration, groundwater recharge, and snow melt, and its wide application in regional and global scale studies. The non-linear soil moisture accounting module of CWatM simulates unsaturated zone flow using the Richards equation with the Van Genuchten simplification (Van Genuchten, 1980). The lumped parameter models–GR4J (Perrin et al., 2003), HyMod (Moore, 1985), and HBV<sub>EDU</sub> (Aghakouchak and Habib, 2010)–were selected for their simple structure, the same input data requirement, small number of model parameters (<8), and their common use in climate change impact studies focusing on river discharge.

Two CWatM models (Burek et al., 2020) were used, which required information on landcover and soil hydraulic properties. These two models differed in the used soil hydraulic properties: one model used data from the Harmonized World Soil Database 1.2. (referred to as CWatM C model), while the other used the same soil hydraulic properties as the HYDRUS-1D model (referred to as CWatM C\* model) (see Supplementary material, Figure S4). The lumped-parameter models and the CWatM model utilized data with a daily temporal resolution. Additionally, the CWatM model employed a spatial resolution of 1 × 1 km<sup>2</sup>. A more detailed description of the models is available in the Supplementary material.

Meteorological data (including precipitation, temperature, wind, relative humidity, and solar radiation) for the Gulling catchment was obtained from the Spartacus dataset in the form of 1 × 1 km gridded datasets for the period between 1990–2016 (Hiebl and Frei, 2016, 2018). Discharge data for the Gulling river was collected from the Aigen station, which is operated and made available by the Central Hydrographical Bureau (HZB; <https://ehyd.gv.at/>, last access: 17 March 2023). The land cover information was obtained from the EU CORINE Land Cover (2018) and the soil map from the Harmonized World Soil Database 1.2.

The catchment-scale modeling workflow consisted of the following steps:

1. Calibration of CWatM using historical climate and discharge data.
2. Calibration of the lumped-parameter models, utilizing catchment averaged PET, rainfall, and snowmelt (from CWatM) along with discharge data.
3. Adjustment of PET to reflect different  $\Delta T$  and  $\Delta CO_2$  scenarios.
4. Execution of climate change scenarios across all models.

Our main focus in employing the rainfall–runoff models was to determine how changes in PET affect water fluxes at the catchment scale and to understand how model choice and complexity influence the sensitivity of these fluxes to changes in PET. Thus, to improve comparability between models, we utilized the same catchment averaged rainfall, snowmelt and PET values computed by the CWatM model for all the rainfall–runoff models. As the catchment consisted of approximately 50% grassland and 50%

forest, we computed PET for each landcover type as follows. For grassland areas, PET in the CWatM model was calculated using the Penman–Monteith equation with stomatal resistance values calibrated from Section 2.4. For forest and other land cover types, we used the FAO-56 Penman–Monteith equation for a well-watered grass reference crop (Allen et al., 1998). Given the current understanding about the sensitivity of ET of spruce and pine forests (Ward et al., 2018), which are the dominant forest type in the catchment, to elevated CO<sub>2</sub> concentrations, we assumed forest areas to be non-sensitive to elevated CO<sub>2</sub>. Finally, to generate an average PET value for each grid cell in the CWatM model, we multiplied the estimated PET for grassland or non-grassland areas by the corresponding land cover fraction from the CORINE Land Cover map. For the analysis at the catchment level, we assumed an LAI of 2.2 for grassland, which is consistent with the calculations at the plot level.

Calibration followed a split-sample approach: the first seven years were allocated for the warm-up period, the next ten years (1997–2006) for validation, and the last ten years (2007–2016) for calibration. The CWatM calibration employs the DEAP framework in Python (Fortin et al., 2012), implementing the NSGA-II evolutionary algorithm (Deb et al., 2002). We used a modified Kling-Gupta efficiency (KGE) metric defined by Kling et al. (2012) and implemented in CWatM (Burek et al., 2020). Additionally, the lumped-parameter models were calibrated using the DREAM algorithm (Vrugt, 2016), which is compatible with a modified KGE metric by Liu et al. (2022). This choice was due to the metric's compatibility with the Bayesian framework used in DREAM. The rainfall–runoff models' calibration was based on daily discharge. The performance of the rainfall–runoff models was analyzed by employing the KGE for overall and high flows and log-transformed KGE (logKGE) for low flow performance (Gauch et al., 2023).

### 2.5.2. Analysis of change of the modeled climate change scenarios

Using one plot and 5 different rainfall–runoff models, we simulated three climate change scenarios reflecting the lysimeter treatments and corresponding to the RCP 6.0 scenario (see Supplementary material, Figure S5; Van Vuuren et al., 2011):

1. warming of 3 °C ( $\Delta T$  scenario);
2. an increase in CO<sub>2</sub> concentration of 300 ppm ( $\Delta CO_2$  scenario);
3. warming of 3 °C combined with an increase in CO<sub>2</sub> concentration of 300 ppm ( $\Delta CT$  scenario)

The relative sensitivity of water fluxes to  $\Delta T$  and  $\Delta CO_2$ , was represented as relative changes between the climate change scenarios water flux and the ambient conditions. In these scenarios, only the input PET was altered, with precipitation unchanged. At the catchment scale, we assessed the effects on ET<sub>a</sub>, GWR, and river discharge. Since each rainfall–runoff model includes a different soil storage component, percolation was calculated internally as the water exiting the soil storage. Given that our calculations included annual fluxes, we assumed all percolation to eventually contribute to groundwater recharge. To account for local climate variability and to compare plot and catchment models, all models used meteorological data from 1990 to 2016.

The  $\Delta CT$  scenario, being the most realistic rather than purely mechanistic, was employed in a detailed examination of its impacts on river discharge (Q), focusing on high (95th percentile,  $\Delta Q_{95}$ ) and low flows (5th percentile,  $\Delta Q_5$ ). Additionally, their relationship with the aridity index (AI), computed as annual precipitation divided with PET, was assessed.

## 3. Results

### 3.1. Observed changes in lysimeter water fluxes

The lysimeter water fluxes, shown in Fig. 3, revealed distinct effects of  $\Delta CO_2$  and  $\Delta T$ . Specifically,  $\Delta CO_2$  led to a general decrease in actual evapotranspiration (ET<sub>a</sub>) by  $-6 \pm 4\%$  and an increase in groundwater recharge (GWR) by  $17 \pm 17\%$  from 2016 to 2021. In contrast,  $\Delta T$  resulted in an increase in ET<sub>a</sub> by  $17 \pm 8\%$  and a decrease in GWR by  $-47 \pm 19\%$ . When both  $\Delta T$  and  $\Delta CO_2$  were present ( $\Delta CT$ ), the influence of  $\Delta T$  prevailed against  $\Delta CO_2$ , causing an increase in ET<sub>a</sub> by  $9 \pm 9\%$  and a decrease in GWR by  $-40 \pm 18\%$ . Notably, both  $\Delta T$  and  $\Delta CT$  were associated with reduced precipitation, primarily due to a decline in non-rainfall water (dew and fog) by  $-5 \pm 2\%$ , while  $\Delta CO_2$  slightly increased precipitation by  $2 \pm 4\%$ . Changes in non-rainfall due to  $\Delta T$  and  $\Delta CO_2$  are explained in greater detail in Forstner et al. (2023). Changes in soil water storage during the growing season ( $\Delta S$ ), were most pronounced due to  $\Delta T$  in 2018, followed by 2019 and 2020 (Fig. 3d). The  $\Delta T$  lysimeters showed the largest changes in  $\Delta S$ , contrasting with minimal changes in the  $\Delta CO_2$  lysimeters, which exhibited the smallest differences in  $\Delta S$ . These observations are consistent with Forstner et al. (2021), who analyzed the same dataset for the period 2015–2018.

ANOVA and post-hoc Tukey tests conducted on daily ET<sub>a</sub> and GWR showed significant differences ( $p < 0.05$ ) among the groups (Ambient [Amb],  $\Delta CO_2$ ,  $\Delta CT$ ,  $\Delta T$ ), except for the comparison between  $\Delta CT$  and the ambient lysimeter. Interestingly, when the dry years of 2018 and 2019 were excluded from the ANOVA analysis, a significant difference emerged between these two groups as well.

### 3.2. Implication of the $\Delta T$ and $\Delta CO_2$ effects in the Penman-Monteith equation

When comparing ET<sub>a</sub> measurements from lysimeters, under non-water-limited conditions, to estimates derived with the Penman–Monteith equation, we found that lysimeters treated with elevated CO<sub>2</sub> exhibited higher stomatal resistance values ( $103 \pm 14 \text{ s m}^{-1}$ ), compared to those without CO<sub>2</sub> treatment ( $71 \pm 14 \text{ s m}^{-1}$ ) (Fig. 4,c). To generalize these findings and compute PET at any CO<sub>2</sub> concentration, we calibrated the CO<sub>2</sub>-adjusted stomatal resistance model, as per Eq. (3). The calibrated values were  $65 \pm 7 \text{ s m}^{-1}$  for the reference stomatal resistance at 300 ppm and  $0.002 \text{ ppm}^{-1}$  for the relative sensitivity of stomatal resistance to CO<sub>2</sub>. The ANOVA analysis on the measured LAI data from 2016 to 2021 indicated no significant effects (Fig. 4,b) of  $\Delta T$  or  $\Delta CO_2$  on LAI,



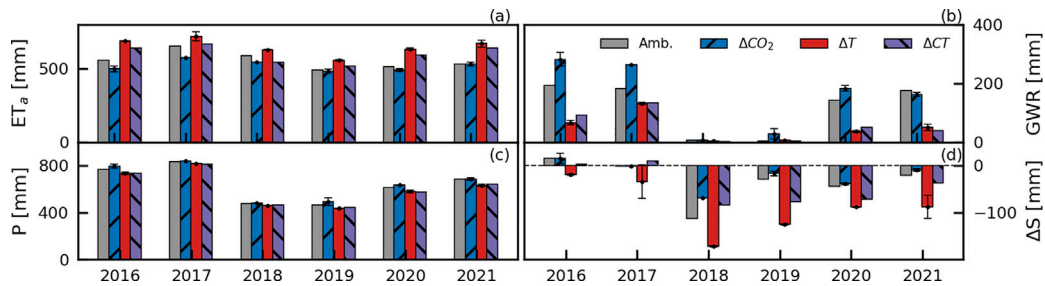


Fig. 3. Absolute values of actual evapotranspiration ( $ET_a$ ; a), groundwater recharge (GWR; b), precipitation (P; c), and the change in soil water storage ( $\Delta S$ ; d) for each of the growing seasons from 2016 to 2021.

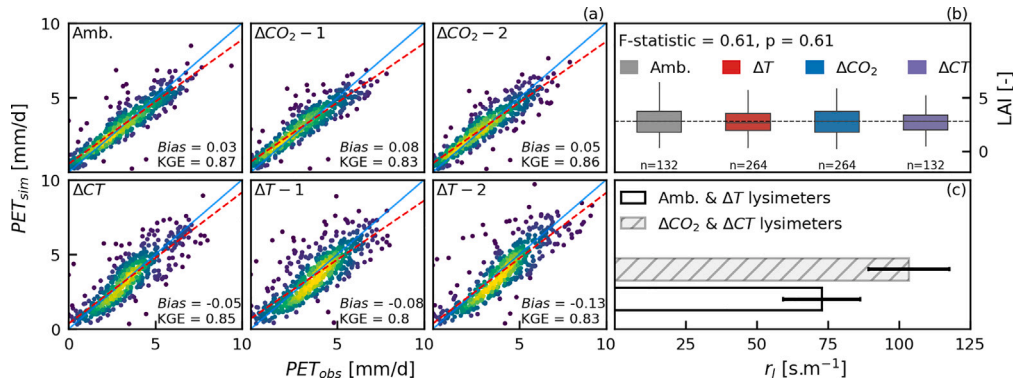


Fig. 4. Scatterplots comparing the potential evapotranspiration observed at the lysimeters ( $PET_{obs}$ ) with the estimated PET using the adapted Penman–Monteith equation ( $PET_{sim}$ ; a). The box plots display the leaf area index (LAI) for each treatment, including ANOVA results (b). The estimated stomatal resistance obtained from inverse modeling for lysimeters under ambient  $CO_2$  and  $\Delta CO_2$  conditions is presented as a bar plot in panel (c).

suggesting that the changes in ET due to  $\Delta CO_2$  were primarily driven by stomatal resistance change. We then applied the  $CO_2$ -adjusted Penman–Monteith equation, with estimated stomatal resistance and sensitivity specific to our grassland site, to validate estimated PET for each lysimeter. The model performance was robust for all lysimeters, as indicated by KGE higher than 0.8 and minimal model biases (Fig. 4,a).

### 3.3. Observed versus modeled changes in water fluxes due to $\Delta T$ and $\Delta CO_2$ at the plot scale

The calibrated HYDRUS-1D model showed good performance in simulating the water fluxes of the ambient lysimeter, as indicated by a KGE of 0.83 for groundwater recharge and a KGE higher than 0.75 for soil water content (see Supplementary material, Figures S1-S3). Fig. 5 presents the model’s sensitivity to  $\Delta T$  and  $\Delta CO_2$ , illustrating relative changes in annual water fluxes between the climate change scenarios and ambient conditions for both modeled data (HYDRUS-1D; 1997–2016) and observed data (lysimeters; 2016–2021). Despite covering different periods, the modeled water fluxes exhibited similar mean annual sensitivity to  $\Delta T$  and  $\Delta CO_2$  as the lysimeters; though the lysimeter data showed greater annual variability (Fig. 5).

For  $\Delta CO_2$ , sensitivities of simulated and observed PET were  $-6 \pm 0.5\%$  and  $-6 \pm 5\%$ , respectively. Under  $\Delta T$ , they were  $17 \pm 2\%$  for simulated and  $18 \pm 8\%$  for observed PET. For  $\Delta CT$ , the sensitivities were  $10 \pm 1\%$  in the simulated data and  $10 \pm 10\%$  in the observed data. Similarly, the sensitivities of both simulated and observed actual evapotranspiration ( $ET_a$ ) to  $\Delta CO_2$  were  $-6 \pm 0.5\%$  and  $-5 \pm 5\%$ , to  $\Delta T$  were  $16 \pm 2\%$  and  $17 \pm 8\%$ , and to  $\Delta CT$  were  $10 \pm 1\%$  and  $9 \pm 10\%$ . Lastly, the sensitivities of GWR to these changes were  $12 \pm 6\%$  and  $8 \pm 11\%$  for  $\Delta CO_2$ ,  $-31 \pm 10\%$  and  $-28 \pm 19\%$  for  $\Delta T$ , and  $-19 \pm 1\%$  and  $-25 \pm 20\%$  for  $\Delta CT$ .

### 3.4. Modeled changes in water fluxes at the catchment scale

#### 3.4.1. Performance of the rainfall–runoff models to simulate river discharge

Performance metrics for both the calibration ( $KGE_{cal}$ , 2007–2016) and validation period ( $KGE_{val}$ , 1997–2006) indicated strong model performance, with KGE values exceeding 0.8 (Table 1). Notably, the CWatM and GR4J models performed particularly well in capturing low flows, indicating their robustness in varied flow conditions, while the HBV and Hymod models were less effective in capturing low flow dynamics.

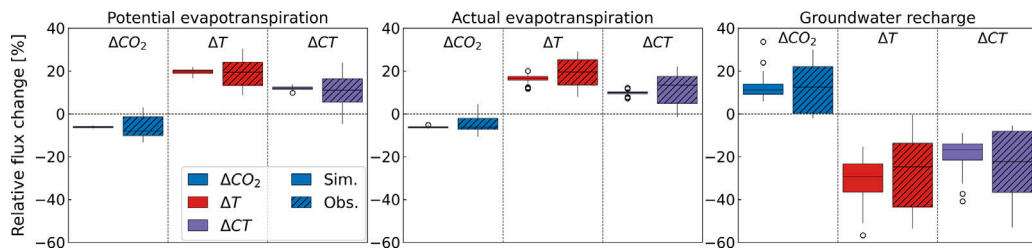


Fig. 5. Annual observed and modeled relative changes in potential evapotranspiration, actual evapotranspiration, and groundwater recharge at the plot scale. The box plots show the annual variability in the relative change of the water flux between the climate change scenario and ambient conditions, for observed fluxes between 2016–2021 and modeled fluxes between 1997–2016.

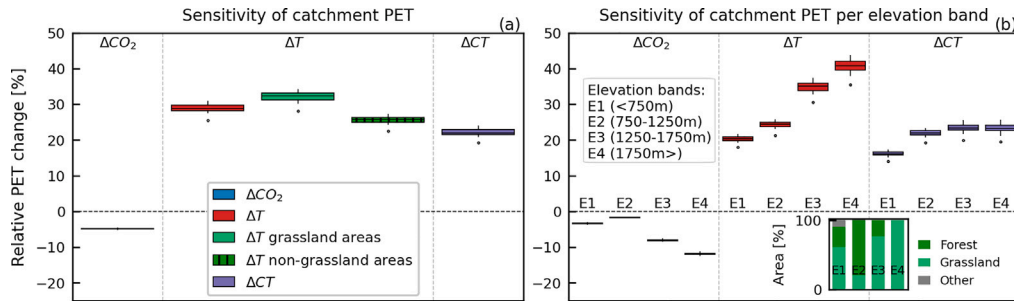


Fig. 6. Box plots illustrating the annual relative change in estimated catchment-averaged PET between the climate change scenarios and ambient conditions (a), and the relative average catchment PET change per elevation band within the catchment for these same scenarios (b).

Table 1

Kling-Gupta efficiency (KGE) and KGE in logarithmic space (logKGE) for all rainfall–runoff models. CWatM (C) model used soil hydraulic properties from the Harmonized World Soil Database 1.2, while CWatM (C\*) used soil hydraulic properties obtained from the ambient lysimeter.

Model	$KGE_{cal}^{val}$	$KGE_{val}^{val}$	$logKGE_{cal}^{val}$	$logKGE_{val}^{val}$
GR4J	0.85	0.80	0.85	0.79
HBV <sub>EDU</sub>	0.85	0.83	0.73	0.60
HyMod	0.84	0.83	0.45	0.4
CWatM (C)	0.80	0.84	0.75	0.81
CWatM* (C*)	0.80	0.82	0.68	0.75

### 3.4.2. Potential evapotranspiration

The analysis demonstrated that annual catchment-scale PET was influenced by both  $\Delta T$  and  $\Delta CO_2$  during the modeled period from 1997 to 2016 (Fig. 6).  $\Delta T$  led to an increase in annual PET of  $30 \pm 1\%$  compared to ambient conditions, while  $\Delta CO_2$  resulted in a reduction of  $-5 \pm 0.1\%$ . Under the  $\Delta CT$  scenario, there was a mean increase in PET of about  $23 \pm 1\%$ . As detailed in Section 2.4, evapotranspiration for the catchment was calculated separately for grassland and non-grassland areas, with each grid cell’s results aggregated according to their respective landcover fractions. Notably, the estimated PET for grassland areas showed greater sensitivity to  $\Delta T$  ( $32 \pm 1\%$ ) compared to the FAO-56 equation ( $27 \pm 1\%$ ) used for non-grassland areas. Additionally, we found that its sensitivity to both  $\Delta T$  and  $\Delta CO_2$  intensifies with increasing elevation. This trend was further clarified through a simple sensitivity analysis presented in Figure S6 in the Supplementary material. The analysis reveals that PET becomes more sensitive to increases in  $\Delta T$  under conditions of lower temperatures and higher wind speeds, which are typical at higher altitudes.

### 3.4.3. Impact on actual ET, groundwater recharge and river discharge

The results of the catchment-scale modeling show that  $\Delta T$  increases  $ET_a$  and decreases GWR and discharge across all models, while  $\Delta CO_2$  has the opposite minor effect (Fig. 7). These models consistently showed the same direction of sensitivity for all fluxes: a mean change in  $ET_a$  of  $-4 \pm 1\%$  for  $\Delta CO_2$ ,  $24 \pm 4\%$  under  $\Delta T$ , and  $19 \pm 3\%$  for  $\Delta CT$ . Similarly, GWR and discharge sensitivities were closely aligned, with increases of  $2 \pm 1\%$  under  $\Delta CO_2$  and decreases of  $-12 \pm 3\%$  under  $\Delta T$  and  $-10 \pm 3\%$  for  $\Delta CT$  for GWR. Discharge sensitivity to  $\Delta CO_2$  was  $2 \pm 0.4\%$ ,  $-11 \pm 2\%$  under  $\Delta T$ , and  $-9 \pm 2\%$  for  $\Delta CT$ .

While the direction of change was consistent across all models, the magnitude of relative sensitivity varied, particularly under the  $\Delta T$  and  $\Delta CT$  scenarios. Notable inter-model differences were observed, especially for the  $ET_a$  flux under  $\Delta T$ , with the HBV<sub>EDU</sub> and CWatM models showing mean relative changes of  $20 \pm 1\%$  and  $28 \pm 2\%$ , respectively. In the  $\Delta CT$  scenario, the GR4J model exhibited the greatest decrease in river discharge, whereas the HBV<sub>EDU</sub> model showed the least decrease. The GR4J model demonstrated the

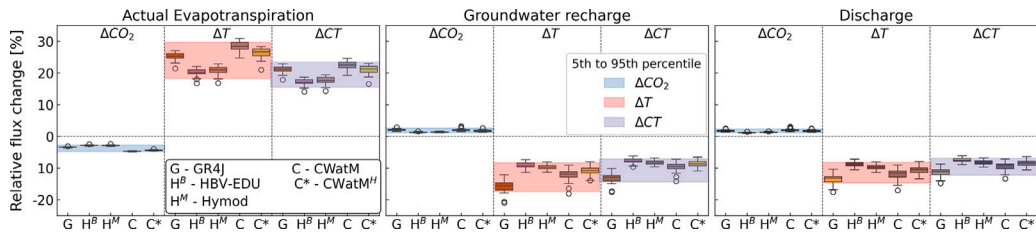


Fig. 7. Modeled relative changes in actual evapotranspiration, groundwater recharge and discharge for GR4J (G), HBV<sub>EDU</sub> (H<sup>B</sup>), HyMod (H<sup>M</sup>), CWatM (C), and CWatM\* (C\*) models. The box plots show the annual variability in the relative change of the flux under the climate scenario and ambient conditions, while the uncertainty bands in each figure represent the 5%–95% range of annual variability in the simulated water flux.

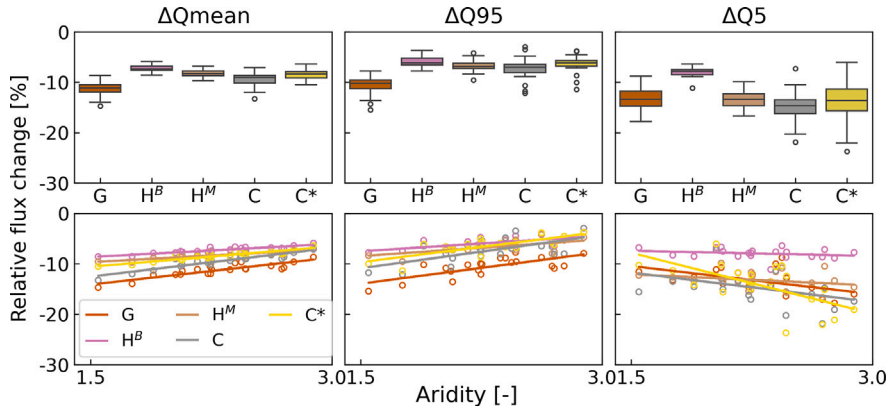


Fig. 8. The upper panels show the relative difference of mean ( $\Delta Q_{mean}$ ), high ( $\Delta Q_{95}$ ) and low ( $\Delta Q_5$ ) flows between the  $\Delta CT$  and the ambient scenario at the catchment scale for GR4J (G), HBV<sub>EDU</sub> (H<sup>B</sup>), HyMod (H<sup>M</sup>), CWatM (C), and CWatM\* (C\*) models. The lower panels of the figure show how the relative change in the flows correlates with the annual aridity index.

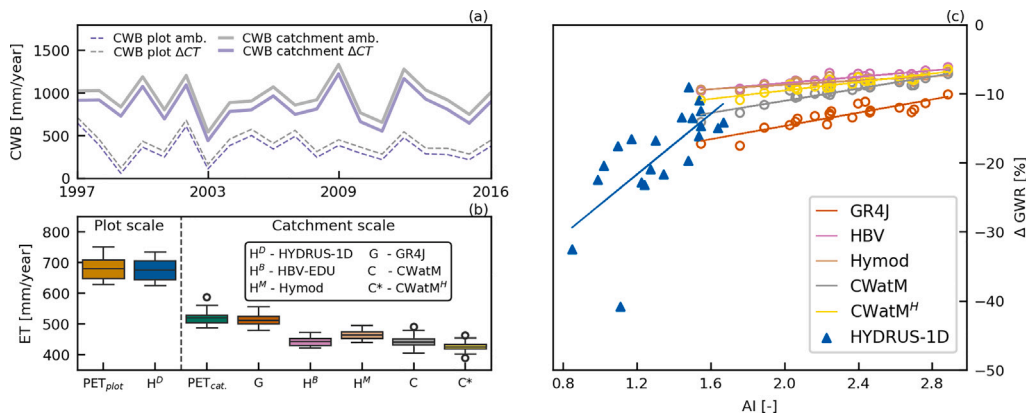


Fig. 9. The calculated annual climatic water balance for the ambient and  $\Delta CT$  scenario (a), the modeled annual PET and  $ET_e$  for the plot and catchment scale (b), the relative change of GWR between ambient conditions and  $\Delta CT$  scenario in relation to aridity for the plot scale, with HYDRUS-1D simulated GWR serving as proxy for lysimeter observations, and at the catchment scale (c).

highest sensitivity in annual river discharge, with a mean relative change of  $-13 \pm 2\%$ , contrasting with the HBV<sub>EDU</sub> model, which had the smallest deviation at  $-9 \pm 1$

### 3.4.4. Sensitivity of extreme flows under elevated CO<sub>2</sub> and warming

The catchment-scale models demonstrated higher sensitivity and greater year-to-year variability for low flows compared to high flows (Fig. 8). When comparing the annual response in discharge across different years to annual aridity, the models consistently showed higher sensitivity of annual mean and high flows in drier conditions. In contrast, the effect of aridity on low flow sensitivity was less clear.

### 3.5. Sensitivity of water fluxes at plot versus catchment scale

The annual catchment-averaged climatic water balance, computed as the difference between annual catchment precipitation and potential evapotranspiration, from 1997 to 2016 was  $590 \pm 165$  mm higher than at the plot scale (Fig. 9,a), indicating that the plot scale was considerably more water-limited than the catchment. This difference can be attributed to both lower precipitation amounts and increased actual evapotranspiration ( $ET_a$ ) at the plot scale (Fig. 9,b), with the latter influenced by its location at a lower elevation compared to the studied catchment. An analysis of groundwater recharge (GWR) sensitivity to aridity shows that both the plot and catchment models are more sensitive during drier years (Fig. 9,c).

## 4. Discussion

### 4.1. Sensitivity of the plot-scale model to climate scenarios

In this study, the Penman–Monteith equation and HYDRUS-1D models showed high performance in replicating lysimeter measurements at the plot level, particularly the soil water content and groundwater recharge in the calibration period (2016–2021) (see Supplementary material, Figure S1). Comparing the longer HYDRUS-1D simulation period (1990–2016) with the lysimeter data, the HYDRUS-1D models accurately reflected the sensitivities of actual evapotranspiration and groundwater recharge to  $\Delta CO_2$  and  $\Delta T$ , consistent with the lysimeter dynamics (Fig. 5). While the models demonstrated comparable sensitivity to climate change variables, they exhibited less year-to-year variability compared to the lysimeter measurements. This difference likely arises because models, as simplifications of the natural system, do not fully capture the complex natural variability found in different lysimeter plots across years (Beven, 2011).

### 4.2. Scaling from plot to catchment: model comparisons and implications

Examining the sensitivity of actual evapotranspiration and groundwater recharge at both plot and catchment scales reveals that at the catchment level, especially in higher elevation areas, actual evapotranspiration shows higher sensitivity. This increase in sensitivity is associated with lower temperatures and higher wind speeds typical of elevated areas. Consequently, shifting from local to catchment scale, particularly in higher elevation areas, leads to a marked increase in actual evapotranspiration sensitivity to  $\Delta T$  and  $\Delta CO_2$ . This aligns with findings from prior studies, supporting the hypothesis that altitude-dependent climate conditions can influence evapotranspiration sensitivity (Guo et al., 2017; Sun et al., 2020).

The sensitivity of groundwater recharge to  $\Delta T$  and  $\Delta CO_2$  is less pronounced at the catchment scale. This could be attributed to the higher amount of precipitation the catchment receives ( $\sim 500$  mm year<sup>-1</sup> greater than plot scale), resulting in more groundwater recharge compared to the plot scale and reduces the impact of potential evapotranspiration. A similar observation was made by other studies (Schübl et al., 2023; Berghuijs et al., 2024), where precipitation dictated the predominant recharge processes. Therefore, at the catchment level, a warmer and more  $CO_2$ -enriched future may result in a significant change in actual evapotranspiration (18%–25% for the  $\Delta CT$ ), but the relative change in discharge may be smaller (10%–15% for the  $\Delta CT$ ). On the other hand, at the plot level, even minor relative changes in actual evapotranspiration could have a larger impact on groundwater recharge.

As described in Section 2.4, our study evaluated the impacts of warming on PET under conditions of constant  $e_a$ , aligning with our lysimeter experiment setup. We also extended our analysis to include PET changes at constant RH, as recommended for studies analyzing the impacts of global warming by Scheff and Frierson (2014). These additional findings, detailed in the Supplementary material (Figure S8), demonstrated a significantly lower sensitivity to warming compared to our lysimeter observations. This complicates direct comparisons at the plot level, and thus was not included in the main text. Furthermore, the sensitivities computed under constant  $e_a$  conditions closely mirrored those reported by other studies in the region. For example, Duethmann and Blöschl (2018) reported similar increases in PET in Austria, observing a 2.8% rise per decade from 1977 to 2014, corresponding to a 0.45 °C temperature increase per decade. This trend suggests a 19% rise in PET with a 3 °C warming—closely reflecting our findings (Fig. 5). Their study, using measured meteorological data including temperature, relative humidity and net radiation, provides a valuable comparison and validates the reliability of our experimental approach. Additionally, our modeled discharge sensitivity aligns with Rhine River discharge projections by Buitink et al. (2021), where a 2.5 °C warming resulted in a 20% reduction in discharge. These similarities indicate that our experimental scenarios were well-aligned with observed regional warming effects. Future research will be better positioned to examine these impacts in more detail when longer time series from lysimeter measurements (Forstner et al., 2021) and eddy covariance data (Pastorello et al., 2020) become available.

When scaling plot findings to the catchment scale, all rainfall–runoff models shared common inputs of rainfall, snowmelt, and PET, and operated on basic groundwater storage assumptions. Despite their differences, the models consistently showed similar patterns in discharge sensitivity and its relationship to water availability. Yet, the sensitivity's magnitude varied, largely due to differing representations of soil water storage and routing mechanisms. These differences affected the calculation of actual evapotranspiration (Fig. 9), impacting both actual evapotranspiration sensitivity, as well as groundwater recharge, and discharge. In line with previous findings (Velázquez et al., 2013; Bastola et al., 2011; Moeck et al., 2016), our findings support the use of multiple models for a more complete evaluation of climate change impacts on water resources, particularly at the catchment level where benchmark data are not available.

These findings highlight the different responses to climate change that emerge when scaling up from plot to catchment level. While these observations may be particularly relevant to mountain catchments like the studied area, where integration across the

whole basin includes inputs from high elevation, high rainfall zones, they also raise important questions about the generalizability of these effects. Further research is needed to understand these dynamics in other types of catchments and under different climatic conditions. This will aid in better predicting the hydrological impacts of climate change and developing effective water resource management strategies for future conditions.

#### 4.3. Increased sensitivity of groundwater recharge and discharge in dry years

In conditions of greater aridity, our study reveals an increased sensitivity of modeled groundwater recharge at both plot and catchment scales, as observed under a future scenario in Fig. 9. The sensitivity becomes more pronounced in drier years, where the reduced total water availability for groundwater recharge or discharge amplifies the response to changes in actual evapotranspiration. However, as opposed to the mean and high flow ( $\Delta Q_{95}$ ), the low flows ( $\Delta Q_5$ ) tend to be less sensitive in dry years (low aridity index in Fig. 8). This corresponds to the expectation that the relationship reverses when water availability limits the effect of  $\Delta T$  on ET, and consequently on GWR and Q. Conversely, under drier conditions with higher temperatures and global radiation, actual evapotranspiration can increase if water availability is not the limiting factor. This phenomenon, known as the drought paradox, leads to amplified decreases in groundwater recharge and river discharge (Mastrotheodoros et al., 2020).

These observations in montane grassland, which are generally energy-limited, highlight the interplay between temperature, evapotranspiration and available water resources, which has important implications for these ecosystems. Shifts in these factors can alter the balance between energy and water availability, leading to shifts in ecosystem dynamics. For example, variations in the annual distribution of precipitation could lead to ecosystems transitioning from energy-limited to water-limited conditions during periods of drought and high temperature (Haslinger et al., 2022; Teuling, 2018), suggesting that future actual evapotranspiration under a warmer climate might be constrained by source limitation (water) or enhanced by source abundance (temperature and radiation).

## 5. Summary and conclusion

In this study, we investigated how climate change could impact the hydrology of montane grassland. We specifically focused on how sensitive plot and catchment water fluxes were to changes in potential evapotranspiration (PET) due to warming and elevated  $\text{CO}_2$  concentrations. To achieve this, we utilized data from a climate change experiment involving lysimeters subjected to warming ( $\Delta T$ ; +3 °C), elevated  $\text{CO}_2$  conditions ( $\Delta \text{CO}_2$ ; +300 ppm), and a combination of both ( $\Delta CT$ ), to simulate future climate change scenarios. The findings from the lysimeters were modeled using a soil hydrological model and extrapolated to the catchment scale, by employing five different rainfall–runoff models of varying complexity. By adjusting the PET inputs in these models, we were able to simulate changes in actual evapotranspiration ( $\text{ET}_a$ ), as well as the potential impacts of these changes on river discharge (Q) and groundwater recharge (GWR). Our key findings include the following:

1. The soil hydrological models effectively reproduced the lysimeter fluxes-with similar sensitivity to  $\Delta \text{CO}_2$  and  $\Delta T$ ; however, they exhibited less variation from year-to-year.
2.  $\Delta T$  increased  $\text{ET}_a$  and decreased GWR and Q, while  $\Delta \text{CO}_2$  mitigated the effects of  $\Delta T$  at both the plot and catchment scale. At the plot scale,  $\Delta \text{CO}_2$  effects partially buffered the hydrological response of  $\Delta T$ . Thus, overlooking effects of  $\Delta \text{CO}_2$  could lead to overestimating the impacts of climate change.
3. The sensitivity of  $\text{ET}_a$  to  $\Delta T$  was greater at the catchment than at the plot scale, reflecting increased ET sensitivity to warming with higher elevation. In contrast, GWR was more sensitive at the plot scale, attributed to drier conditions at these lower elevations compared to the catchment scale.
4. Drier conditions increased the sensitivity of GWR and Q to  $\Delta CT$  across scales, indicating increased risks in a likely future climate.
5. Despite consistent patterns in water flux sensitivity to  $\Delta T$  and  $\Delta \text{CO}_2$  across different rainfall–runoff models, variability in impact magnitude underscores the value of multi-model approach for more robust climate change impact assessments on water resources.

### CRedit authorship contribution statement

**Matevž Vremec:** Methodology, Formal analysis, Conceptualization. **Peter Burek:** Writing – review & editing, Methodology. **Luca Guillaumot:** Writing – review & editing, Methodology. **Jesse Radolinski:** Writing – review & editing, Methodology. **Veronika Forstner:** Writing – review & editing, Data curation. **Markus Herndl:** Writing – review & editing, Data curation. **Christine Stumpp:** Writing – review & editing, Methodology. **Michael Bahn:** Writing – review & editing, Methodology. **Steffen Birk:** Writing – review & editing, Methodology, Conceptualization.

### Declaration of competing interest

The authors declare that they have no known competing financial interests or personal relationships that could have appeared to influence the work reported in this paper.

## Data availability

Data will be made available on request.

## Acknowledgments

This work was carried out in the framework of the ClimGrassHydro and RechAUT projects funded by the Austrian Academy of Sciences (ÖAW), and the WaterStressAT project funded by the Austrian Climate Research Programme (ACRP). The lysimeter facility and the project 'Lysi-T-FACE' (DaFNE, 100719) at Gumpenstein was funded by the Austrian Federal Ministry of Agriculture, Forestry, Environment and Water Management (BMLFUW). Meteorological data was provided by the Central Institution for Meteorology and Geodynamics (ZAMG, now Geosphere Austria, Vienna, Austria), Vienna, Austria. We would further thank our colleagues Martina Schink, Andreas Klingler, Andreas Schaumberger, Matthias Kandolf, Medardus Schweiger and Erich Pötsch at the corresponding lysimeter station for their support. The authors acknowledge the financial support by the University of Graz.

## Appendix A. Supplementary data

Supplementary material related to this article can be found online at <https://doi.org/10.1016/j.ejrh.2024.101970>.

## References

- Aghakouchak, A., Habib, E., 2010. Application of a conceptual hydrologic model in teaching hydrologic processes. pp. 963–973.
- Allan, R.P., Barlow, M., Byrne, M.P., Cherchi, A., Douville, H., Fowler, H.J., Gan, T.Y., Pendergrass, A.G., Rosenfeld, D., Swann, A.L.S., Wilcox, L.J., Zolina, O., 2020. Advances in understanding large-scale responses of the water cycle to climate change. *Ann. New York Acad. Sci.* 1472 (1), 49–75. <https://dx.doi.org/10.1111/nyas.14337>, URL <https://onlinelibrary.wiley.com/doi/10.1111/nyas.14337>.
- Allen, R.G., Pereira, L.S., Raes, D., Smith, M., et al., 1998. *Crop Evapotranspiration-Guidelines for Computing Crop Water Requirements-FAO Irrigation and Drainage Paper 56*. Vol. 300, Fao, Rome, p. D05109.
- Bastola, S., Murphy, C., Sweeney, J., 2011. The role of hydrological modelling uncertainties in climate change impact assessments of Irish river catchments. *Adv. Water Resour.* 34 (5), 562–576. <https://dx.doi.org/10.1016/j.advwatres.2011.01.008>, URL <https://linkinghub.elsevier.com/retrieve/pii/S0309170811000224>.
- Berg, A., Findell, K., Lintner, B., Giannini, A., Seneviratne, S.I., Van Den Hurk, B., Lorenz, R., Pitman, A., Hagemann, S., Meier, A., Cheruy, F., Ducharme, A., Malyshev, S., Milly, P.C.D., 2016. Land-atmosphere feedbacks amplify aridity increase over land under global warming. *Nature Clim. Change* 6 (9), 869–874. <https://dx.doi.org/10.1038/nclimate3029>, URL <https://www.nature.com/articles/nclimate3029>.
- Berghuijs, W.R., Collenteur, R.A., Jasechko, S., Jaramillo, F., Luijendijk, E., Moeck, C., Van Der Velde, Y., Allen, S.T., 2024. Groundwater recharge is sensitive to changing long-term aridity. *Nature Clim. Change* 14 (4), 357–363. <https://dx.doi.org/10.1038/s41558-024-01953-z>, URL <https://www.nature.com/articles/s41558-024-01953-z>.
- Beven, K.J., 2011. *Rainfall-Runoff Modelling: The Primer*. John Wiley & Sons.
- BMLRT, R., 2020. *Grüner Bericht 2020 - Bericht über die situation der österreichischen land- und forstwirtschaft*. Technical Report, Bundesminist. Für Nachhalt. Tour., Wien, p. 297 S.
- Broderick, C., Matthews, T., Wilby, R.L., Bastola, S., Murphy, C., 2016. Transferability of hydrological models and ensemble averaging methods between contrasting climatic periods: Model transferability. *Water Resour. Res.* 52 (10), 8343–8373. <https://dx.doi.org/10.1002/2016WR018850>, URL <http://doi.wiley.com/10.1002/2016WR018850>.
- Buitink, J., Melsen, L.A., Teuling, A.J., 2021. Seasonal discharge response to temperature-driven changes in evaporation and snow processes in the Rhine Basin. *Earth Syst. Dyn.* 12 (2), 387–400. <https://dx.doi.org/10.5194/esd-12-387-2021>, URL <https://esd.copernicus.org/articles/12/387/2021/>.
- Burek, P., Satoh, Y., Kahl, T., Tang, T., Greve, P., Smilovic, M., Guillaumont, L., Zhao, F., Wada, Y., 2020. Development of the Community Water Model (CWatM v1.04) – a high-resolution hydrological model for global and regional assessment of integrated water resources management. *Geosci. Model Dev.* 13 (7), 3267–3298. <https://dx.doi.org/10.5194/gmd-13-3267-2020>, URL <https://gmd.copernicus.org/articles/13/3267/2020/>.
- Deb, K., Pratap, A., Agarwal, S., Meyarivan, T., 2002. A fast and elitist multiobjective genetic algorithm: NSGA-II. *IEEE Trans. Evol. Comput.* 6 (2), 182–197. <https://dx.doi.org/10.1109/4235.996017>, URL <http://ieeexplore.ieee.org/document/996017/>.
- Douville, H., Willett, K.M., 2023. A drier than expected future, supported by near-surface relative humidity observations. *Sci. Adv.* 9 (30), eade6253. <https://dx.doi.org/10.1126/sciadv.ade6253>, URL <https://www.science.org/doi/10.1126/sciadv.ade6253>.
- Duethmann, D., Blöschl, G., 2018. Why has catchment evaporation increased in the past 40 years? A data-based study in Austria. *Hydrol. Earth Syst. Sci.* 22 (10), 5143–5158. <https://dx.doi.org/10.5194/hess-22-5143-2018>, URL <https://hess.copernicus.org/articles/22/5143/2018/>.
- Duethmann, D., Blöschl, G., Parajka, J., 2020. Why does a conceptual hydrological model fail to correctly predict discharge changes in response to climate change? *Hydrol. Earth Syst. Sci.* 24 (7), 3493–3511. <https://dx.doi.org/10.5194/hess-24-3493-2020>, URL <https://hess.copernicus.org/articles/24/3493/2020/>.
- Ernst, P., Loeper, E.G., 1976. *Temperaturentwicklung und Vegetationsbeginn auf dem Grunland*. *Wirtsch. Futter*.
- Faticchi, S., Pappas, C., Ivanov, V.Y., 2016. Modeling plant–water interactions: an ecohydrological overview from the cell to the global scale. *WIREs Water* 3 (3), 327–368. <https://dx.doi.org/10.1002/wat2.1125>, URL <https://onlinelibrary.wiley.com/doi/10.1002/wat2.1125>.
- Forstner, V., Groh, J., Vremec, M., Herndl, M., Vereecken, H., Gerke, H.H., Birk, S., Pütz, T., 2021. Response of water fluxes and biomass production to climate change in permanent grassland soil ecosystems. *Hydrol. Earth Syst. Sci.* 25 (12), 6087–6106. <https://dx.doi.org/10.5194/hess-25-6087-2021>, URL <https://hess.copernicus.org/articles/25/6087/2021/>.
- Forstner, V., Vremec, M., Herndl, M., Birk, S., 2023. Effects of dry spells on soil moisture and yield anomalies at a montane managed grassland site: A lysimeter climate experiment. *Ecohydrology* <https://dx.doi.org/10.1002/eco.2518>, URL <https://onlinelibrary.wiley.com/doi/10.1002/eco.2518>.
- Fortin, F.A., De Rainville, F.M., Gardner, M., Parizeau, M., Gagné, C., 2012. *DEAP: Evolutionary Algorithms Made Easy*. Vol. 13, pp. 2171–2175.
- Gauch, M., Kratzert, F., Gilon, O., Gupta, H., Mai, J., Nearing, G., Tolson, B., Hochreiter, S., Klotz, D., 2023. In defense of metrics: Metrics sufficiently encode typical human preferences regarding hydrological model performance. *Water Resour. Res.* 59 (6), e2022WR033918. <https://dx.doi.org/10.1029/2022WR033918>, URL <https://agupubs.onlinelibrary.wiley.com/doi/10.1029/2022WR033918>.
- Green, T.R., Taniguchi, M., Kooi, H., Gurdak, J.J., Allen, D.M., Hiscock, K.M., Treidel, H., Aureli, A., 2011. Beneath the surface of global change: Impacts of climate change on groundwater. *J. Hydrol.* 405 (3–4), 532–560. <https://dx.doi.org/10.1016/j.jhydrol.2011.05.002>, URL <https://linkinghub.elsevier.com/retrieve/pii/S0022169411002988>.
- Guo, D., Westra, S., Maier, H.R., 2017. Sensitivity of potential evapotranspiration to changes in climate variables for different Australian climatic zones. *Hydrol. Earth Syst. Sci.* 21 (4), 2107–2126. <https://dx.doi.org/10.5194/hess-21-2107-2017>, URL <https://hess.copernicus.org/articles/21/2107/2017/>.

- Hanus, S., Hrachowitz, M., Zekollari, H., Schoups, G., Vizcaino, M., Kaitna, R., 2021. Future changes in annual, seasonal and monthly runoff signatures in contrasting Alpine catchments in Austria. *Hydrol. Earth Syst. Sci.* 25 (6), 3429–3453. <http://dx.doi.org/10.5194/hess-25-3429-2021>, URL <https://hess.copernicus.org/articles/25/3429/2021/>.
- Haslinger, K., Schöner, W., Abermann, J., Laaha, G., Andre, K., Olefs, M., Koch, R., 2022. Contradictory Signal in Future Surface Water Availability in Austria: Increase on Average Vs. Higher Probability of Droughts. preprint, Atmospheric, Meteorological and Climatological Hazards, <http://dx.doi.org/10.5194/egusphere-2022-191>, URL <https://egusphere.copernicus.org/preprints/2022/egusphere-2022-191/>.
- Herndl, M., Pötsch, E., Bohner, A., Kandolf, M., 2011. Lysimeter als Bestandteil eines technischen Versuchskonzeptes zur Simulation der Erderwärmung im Grünland. In: Bericht LFZ Raumberg-Gumpenstein, 14. Gumpensteiner Lysimetertagung "Lysimeter in Der Klimafolgenforschung". ISBN-13: 978-3-902559-61-6. pp. 119–126.
- Hiebl, J., Frei, C., 2016. Daily temperature grids for Austria since 1961—concept, creation and applicability. *Theor. Appl. Climatol.* 124 (1), 161–178. <http://dx.doi.org/10.1007/s00704-015-1411-4>, Publisher: Springer.
- Hiebl, J., Frei, C., 2018. Daily precipitation grids for Austria since 1961—development and evaluation of a spatial dataset for hydroclimatic monitoring and modelling. *Theor. Appl. Climatol.* 132 (1–2), 327–345. <http://dx.doi.org/10.1007/s00704-017-2093-x>, URL <https://link.springer.com/10.1007/s00704-017-2093-x>.
- Houska, T., Kraft, P., Chamorro-Chavez, A., Breuer, L., 2015. SPOTting model parameters using a ready-made python package. *PLoS One* 10, 1–22. <http://dx.doi.org/10.1371/journal.pone.0145180>, Publisher: Public Library of Science.
- Inauen, N., Körner, C., Hiltbrunner, E., 2013. Hydrological consequences of declining land use and elevated CO<sub>2</sub> in alpine grassland. In: Bardgett, R. (Ed.), *J. Ecol.* 101 (1), 86–96. <http://dx.doi.org/10.1111/1365-2745.12029>, URL <https://onlinelibrary.wiley.com/doi/10.1111/1365-2745.12029>.
- IPCC, 2021. The physical science basis. Contribution of Working Group I to the sixth assessment report of the intergovernmental panel on climate change. In: *Climate Change 2021*. Cambridge University Press.
- Karlsson, I.B., Sonnenborg, T.O., Refsgaard, J.C., Trolle, D., Børgesen, C.D., Olesen, J.E., Jeppesen, E., Jensen, K.H., 2016. Combined effects of climate models, hydrological model structures and land use scenarios on hydrological impacts of climate change. *J. Hydrol.* 535, 301–317. <http://dx.doi.org/10.1016/j.jhydrol.2016.01.069>, URL <https://linkinghub.elsevier.com/retrieve/pii/S0022169416300099>.
- Kimball, B.A., 2005. Theory and performance of an infrared heater for ecosystem warming. *Global Change Biol.* 11 (11), 2041–2056. <http://dx.doi.org/10.1111/j.1365-2486.2005.1028.x>, URL <https://onlinelibrary.wiley.com/doi/10.1111/j.1365-2486.2005.1028.x>.
- Kling, H., Fuchs, M., Paulin, M., 2012. Runoff conditions in the upper Danube basin under an ensemble of climate change scenarios. *J. Hydrol.* 424–425, 264–277. <http://dx.doi.org/10.1016/j.jhydrol.2012.01.011>, URL <https://linkinghub.elsevier.com/retrieve/pii/S0022169412000431>.
- Leakey, A.D.B., Ainsworth, E.A., Bernacchi, C.J., Rogers, A., Long, S.P., Ort, D.R., 2009. Elevated CO<sub>2</sub> effects on plant carbon, nitrogen, and water relations: six important lessons from FACE. *J. Exp. Botany* 60 (10), 2859–2876. <http://dx.doi.org/10.1093/jxb/erp096>, URL <https://academic.oup.com/jxb/article-lookup/doi/10.1093/jxb/erp096>.
- Liu, Y., Fernández-Ortega, J., Mudarra, M., Hartmann, A., 2022. Pitfalls and a feasible solution for using KGE as an informal likelihood function in MCMC methods: DREAM<sub>(ZS)</sub> as an example. *Hydrol. Earth Syst. Sci.* 26 (20), 5341–5355. <http://dx.doi.org/10.5194/hess-26-5341-2022>, URL <https://hess.copernicus.org/articles/26/5341/2022/>.
- Mastrotheodoros, T., Pappas, C., Molnar, P., Burlando, P., Manoli, G., Parajka, J., Rigon, R., Szeles, B., Bottazzi, M., Hadjidoukas, P., Fatichi, S., 2020. More green and less blue water in the Alps during warmer summers. *Nature Clim. Change* 10 (2), 155–161. <http://dx.doi.org/10.1038/s41558-019-0676-5>, URL <http://www.nature.com/articles/s41558-019-0676-5>.
- Miglietta, F., Hoosbeek, M.R., Foot, J., Gigon, F., Hassinen, A., Heijmans, M., Peressotti, A., Saarinen, T., van Breemen, N., Wallén, B., 2001. Spatial and temporal performance of the MiniFACE (free air CO<sub>2</sub> enrichment) system on bog ecosystems in Northern and central Europe. *Environ. Monit. Assess.* 66 (2), 107–127. <http://dx.doi.org/10.1023/A:1026495830251>.
- Milly, P.C.D., Dunne, K.A., 2016. Potential evapotranspiration and continental drying. *Nature Clim. Change* 6, <http://dx.doi.org/10.1038/nclimate3046>.
- Moeck, C., Brunner, P., Hunkeler, D., 2016. The influence of model structure on groundwater recharge rates in climate-change impact studies. *Hydrogeol. J.* 24 (5), 1171–1184. <http://dx.doi.org/10.1007/s10040-016-1367-1>, URL <http://link.springer.com/10.1007/s10040-016-1367-1>.
- Moore, R.J., 1985. The probability-distributed principle and runoff production at point and basin scales. *Hydrol. Sci. J.* 30 (2), 273–297. <http://dx.doi.org/10.1080/02626668509490989>, URL <http://www.tandfonline.com/doi/abs/10.1080/02626668509490989>.
- Pastorello, G., Trotta, C., Canfora, E., Chu, H., Christianson, D., Cheah, Y.-W., Poindexter, C., Chen, J., Elbashandy, A., Humphrey, M., Isaac, P., Polidori, D., Reichstein, M., Ribeca, A., van Ingen, C., Vuichard, N., Zhang, L., Amiro, B., Ammann, C., Arain, M.A., Ardö, J., Arkebauer, T., Arndt, S.K., Arriga, N., Aubinet, M., Aurela, M., Baldocchi, D., Barr, A., Beamesderfer, E., Marchesini, L.B., Bergeron, O., Beringer, J., Bernhofer, C., Berveiller, D., Billesbach, D., Black, T.A., Blanken, P.D., Bohrer, G., Boike, J., Bolstad, P.V., Bonal, D., Bonnefond, J.-M., Bowling, D.R., Bracho, R., Brodeur, J., Brümmer, C., Buchmann, N., Burban, B., Burns, S.P., Buysse, P., Cale, P., Cavagna, M., Cellier, P., Chen, S., Chini, I., Christensen, T.R., Cleverly, J., Collalti, A., Consalvo, C., Cook, B.D., Cook, D., Coursolle, C., Cremonese, E., Curtis, P.S., D'Andrea, E., da Rocha, H., Dai, X., Davis, K.J., Cinti, B.D., Grandcourt, A.d., Ligne, A.D., De Oliveira, R.C., Delpiere, N., Desai, A.R., Di Bella, C.M., Tommasi, P.d., Dolman, H., Domingo, F., Dong, G., Dore, S., Duce, P., Dufréne, E., Dunn, A., Dušek, J., Eamus, D., Eichelmann, U., ElKhidir, H.A.M., Eugster, W., Ewen, C.M., Ewers, B., Famulari, D., Fares, S., Feigenwinter, I., Feitz, A., Fensholt, R., Filippa, G., Fischer, M., Frank, J., Galvagno, M., Gharun, M., Gianelle, D., Gielen, B., Gioli, B., Gitelson, A., Goded, I., Goeckede, M., Goldstein, A.H., Gough, C.M., Goulden, M.L., Graf, A., Griebel, A., Gruening, C., Grünwald, T., Hammerle, A., Han, S., Han, X., Hansen, B.U., Hanson, C., Hatakka, J., He, Y., Hehn, M., Heinesch, B., Hinko-Najera, N., Hörtnagl, L., Hutley, L., Ibrom, A., Ikawa, H., Jackowicz-Korczynski, M., Janouš, D., Jans, W., Jassal, R., Jiang, S., Kato, T., Khomik, M., Klatt, J., Knohl, A., Knox, S., Kobayashi, H., Koerber, G., Kolle, O., Kosugi, Y., Kotani, A., Kowalski, A., Kruijt, B., Kurbatova, J., Kutsch, W.L., Kwon, H., Launiainen, S., Laurila, T., Law, B., Leuning, R., Li, Y., Liddell, M., Limousin, J.-M., Lion, M., Liska, A.J., Lohila, A., López-Ballesteros, A., López-Blanco, E., Loubet, B., Loustau, D., Lucas-Moffat, A., Lüers, J., Ma, S., Macfarlane, C., Magliulo, V., Maier, R., Mammarella, I., Manca, G., Marcolla, B., Margolis, H.A., Marras, S., Massman, W., Mastezanov, M., Matamala, R., Matthes, J.H., Mazzenga, F., McCaughey, H., McHugh, I., McMillan, A.M.S., Merbold, L., Meyer, W., Meyers, T., Miller, S.D., Minerbi, S., Moderow, U., Monson, R.K., Montagnani, L., Moore, C.E., Moors, E., Moreaux, V., Moureaux, C., Munger, J.W., Nakai, T., Neiryneck, J., Nescic, Z., Nicolini, G., Noormets, A., Northwood, M., Nosenko, M., Nouvellon, Y., Novick, K., Oechel, W., Olesen, J.E., Ormival, J.-M., Papuga, S.A., Parmentier, F.-J., Paul-Limoges, E., Pavelka, M., Peichl, M., Pendall, E., Phillips, R.P., Pilegaard, K., Pirk, N., Posse, G., Powell, T., Prasse, H., Prober, S.M., Rambal, S., Rannik, U., Raz-Yaseef, N., Rebmann, C., Reed, D., Dios, V.R.d., Restrepo-Coupe, N., Reverter, B.R., Roland, M., Sabbatini, S., Sachs, T., Saeska, S.R., Sánchez-Cañete, E.P., Sanchez-Mejia, Z.M., Schmid, H.P., Schmidt, M., Schneider, K., Schrader, F., Schroder, I., Scott, R.L., Sedláč, P., Serrano-Ortiz, P., Shao, C., Shi, P., Shironya, I., Siebcke, L., Šigut, L., Silberstein, R., Sirca, C., Spano, D., Steinbrecher, R., Stevens, R.M., Sturtevant, C., Suyker, A., Tagesson, T., Takanaishi, S., Tang, Y., Tapper, N., Thom, J., Tomassucci, M., Tuovinen, J.-P., Urbanski, S., Valentini, R., van der Molen, M., van Gorsel, E., van Huissteden, K., Varlagin, A., Verfaillie, J., Vesala, T., Vincke, C., Vitale, D., Vygodskaya, N., Walker, J.P., Walter-Shea, E., Wang, H., Weber, R., Westermann, S., Wille, C., Wofsy, S., Wohlfahrt, G., Wolf, S., Woodgate, W., Li, Y., Zampedri, R., Zhang, J., Zhou, G., Zona, D., Agarwal, D., Biraud, S., Torn, M., Papale, D., 2020. The FLUXNET2015 dataset and the ONEFlux processing pipeline for eddy covariance data. *Sci. Data* 7 (1), 225. <http://dx.doi.org/10.1038/s41597-020-0534-3>, URL <https://www.nature.com/articles/s41597-020-0534-3>.
- Perrin, C., Michel, C., Andréassian, V., 2003. Improvement of a parsimonious model for streamflow simulation. *J. Hydrol.* 279 (1–4), 275–289. [http://dx.doi.org/10.1016/S0022-1694\(03\)00225-7](http://dx.doi.org/10.1016/S0022-1694(03)00225-7), URL <https://linkinghub.elsevier.com/retrieve/pii/S0022169403002257>.
- Piepho, H.-P., Herndl, M., Pötsch, E.M., Bahn, M., 2017. Designing an experiment with quantitative treatment factors to study the effects of climate change. *J. Agron. Crop Sci.* 203 (6), 584–592. <http://dx.doi.org/10.1111/jac.12225>, URL <https://onlinelibrary.wiley.com/doi/10.1111/jac.12225>.

- Ritchie, J.T., 1972. Model for predicting evaporation from a row crop with incomplete cover. *Water Resour. Res.* 8 (5), 1204–1213. <http://dx.doi.org/10.1029/WR008i005p01204>, URL <http://doi.wiley.com/10.1029/WR008i005p01204>.
- Schaumberger, A., 2011. Räumliche Modelle zur Vegetations-und Ertragsdynamik im Wirtschaftsgrünland. Dissertation.
- Scheff, J., Frierson, D.M.W., 2014. Scaling potential evapotranspiration with greenhouse warming. *J. Clim.* 27 (4), 1539–1558. <http://dx.doi.org/10.1175/JCLI-D-13-00233.1>, URL <http://journals.ametsoc.org/doi/10.1175/JCLI-D-13-00233.1>.
- Schübl, M., Brunetti, G., Fuchs, G., Stump, C., 2023. Estimating vadose zone water fluxes from soil water monitoring data: a comprehensive field study in Austria. *Hydrol. Earth Syst. Sci.* 27 (7), 1431–1455. <http://dx.doi.org/10.5194/hess-27-1431-2023>, URL <https://hess.copernicus.org/articles/27/1431/2023/>.
- Schübl, M., Stump, C., Brunetti, G., 2022. A Bayesian perspective on the information content of soil water measurements for the hydrological characterization of the vadose zone. *J. Hydrol.* 613, 128429. <http://dx.doi.org/10.1016/j.jhydrol.2022.128429>, URL <https://linkinghub.elsevier.com/retrieve/pii/S0022169422009994>.
- Shen, H., Tolson, B.A., Mai, J., 2022. Time to update the split-sample approach in hydrological model calibration. *Water Resour. Res.* 58 (3), <http://dx.doi.org/10.1029/2021WR031523>, URL <https://onlinelibrary.wiley.com/doi/10.1029/2021WR031523>.
- Shepherd, T.G., 2019. Storyline approach to the construction of regional climate change information. *Proc. R. Soc. A* 475 (2225), 20190013. <http://dx.doi.org/10.1098/rspa.2019.0013>, URL <https://royalsocietypublishing.org/doi/10.1098/rspa.2019.0013>.
- Šimůnek, J., Van Genuchten, M.T., Šejna, M., 2008. Development and applications of the hydrus and stanmod software packages and related codes. *Vadose Zone J.* 7 (2), 587–600. <http://dx.doi.org/10.2136/vzj2007.0077>, URL <https://access.onlinelibrary.wiley.com/doi/10.2136/vzj2007.0077>.
- Stump, C., Stiehler, W., Kandolf, M., Šimůnek, J., 2012. Effects of land cover and fertilization method on water flow and solute transport in five lysimeters: A long-term study using stable water isotopes. *Vadose Zone J.* 11 (1), <http://dx.doi.org/10.2136/vzj2011.0075>, URL <http://doi.wiley.com/10.2136/vzj2011.0075>.
- Sun, J., Wang, G., Sun, X., Lin, S., Hu, Z., Huang, K., 2020. Elevation-dependent changes in reference evapotranspiration due to climate change. *Hydrol. Process.* 34 (26), 5580–5594. <http://dx.doi.org/10.1002/hyp.13978>, URL <https://onlinelibrary.wiley.com/doi/10.1002/hyp.13978>.
- Teuling, A.J., 2018. A hot future for European droughts. *Nature Clim. Change* 8 (5), 364–365. <http://dx.doi.org/10.1038/s41558-018-0154-5>, URL <http://www.nature.com/articles/s41558-018-0154-5>.
- Ukkola, A.M., Prentice, I.C., Keenan, T.F., Van Dijk, A.I.J.M., Viney, N.R., Myneni, R.B., Bi, J., 2016. Reduced streamflow in water-stressed climates consistent with CO2 effects on vegetation. *Nature Clim. Change* 6 (1), 75–78. <http://dx.doi.org/10.1038/nclimate2831>, URL <http://www.nature.com/articles/nclimate2831>.
- Van Genuchten, M.T., 1980. A closed-form equation for predicting the hydraulic conductivity of unsaturated soils. *Soil Sci. Soc. Am. J.* 44 (5), 892–898. <http://dx.doi.org/10.2136/sssaj1980.03615995004400050002x>, URL <http://doi.wiley.com/10.2136/sssaj1980.03615995004400050002x>.
- Van Tiel, M., Weiler, M., Freudiger, D., Moretti, G., Kohn, I., Gerlinger, K., Stahl, K., 2023. Melting alpine water towers aggravate downstream low flows: A stress-test storyline approach. *Earth's Future* 11 (3), e2022EF003408. <http://dx.doi.org/10.1029/2022EF003408>, URL <https://agupubs.onlinelibrary.wiley.com/doi/10.1029/2022EF003408>.
- Van Vuuren, D.P., Edmonds, J., Kainuma, M., Riahi, K., Thomson, A., Hibbard, K., Hurtt, G.C., Kram, T., Krey, V., Lamarque, J.-F., et al., 2011. The representative concentration pathways: an overview. *Clim. Change* 109 (1), 5–31. <http://dx.doi.org/10.1007/s10584-011-0148-z>, Publisher: Springer.
- Velázquez, J.A., Schmid, J., Ricard, S., Muerth, M.J., Gauvin St-Denis, B., Minville, M., Chaumont, D., Caya, D., Ludwig, R., Turcotte, R., 2013. An ensemble approach to assess hydrological models' contribution to uncertainties in the analysis of climate change impact on water resources. *Hydrol. Earth Syst. Sci.* 17 (2), 565–578. <http://dx.doi.org/10.5194/hess-17-565-2013>, URL <https://hess.copernicus.org/articles/17/565/2013/>.
- Virtanen, P., Gommers, R., Oliphant, T.E., Haberland, M., Reddy, T., Cournapeau, D., Burovski, E., Peterson, P., Weckesser, W., Bright, J., van der Walt, S.J., Brett, M., Wilson, J., Millman, K.J., Mayorov, N., Nelson, A.R.J., Jones, E., Kern, R., Larson, E., Carey, C.J., Polat, I., Feng, Y., Moore, E.W., VanderPlas, J., Laxalde, D., Perktold, J., Cimrman, R., Henriksen, I., Quintero, E.A., Harris, C.R., Archibald, A.M., Ribeiro, A.H., Pedregosa, F., van Mulbregt, P., SciPy 1.0 Contributors, 2020. SciPy 1.0: Fundamental algorithms for scientific computing in Python. *Nature Methods* 17, 261–272. <http://dx.doi.org/10.1038/s41592-019-0686-2>.
- Vremec, M., Colletneur, R., Birk, S., 2024. PyEt v1.3.1: a Python package for the estimation of potential evapotranspiration. <http://dx.doi.org/10.5194/gmd-2024-63>, URL <https://gmd.copernicus.org/preprints/gmd-2024-63/>.
- Vremec, M., Forstner, V., Herndl, M., Colletneur, R., Schaumberger, A., Birk, S., 2023. Sensitivity of evapotranspiration and seepage to elevated atmospheric CO2 from lysimeter experiments in a montane grassland. *J. Hydrol.* 617, 128875. <http://dx.doi.org/10.1016/j.jhydrol.2022.128875>, URL <https://linkinghub.elsevier.com/retrieve/pii/S0022169422014457>.
- Vremec, M., Klingler, A., Herndl, M., Schaumberger, A., Birk, S., 2021. Estimating crop evapotranspiration of managed alpine grassland using remotely sensed LAI.
- Vrugt, J.A., 2016. Markov chain Monte Carlo simulation using the DREAM software package: Theory, concepts, and MATLAB implementation. *Environ. Model. Softw.* 75, 273–316. <http://dx.doi.org/10.1016/j.envsoft.2015.08.013>, URL <https://linkinghub.elsevier.com/retrieve/pii/S1364815215300396>.
- Wagner, T., Themeßl, M., Schüppel, A., Gobiet, A., Stigler, H., Birk, S., 2017. Impacts of climate change on stream flow and hydro power generation in the Alpine region. *Environ. Earth Sci.* 76 (1), 4. <http://dx.doi.org/10.1007/s12665-016-6318-6>.
- Ward, E.J., Oren, R., Seok Kim, H., Kim, D., Tor-ngern, P., Ewers, B.E., McCarthy, H.R., Oishi, A.C., Pataki, D.E., Palmroth, S., Phillips, N.G., Schäfer, K.V.R., 2018. Evapotranspiration and water yield of a pine-broadleaf forest are not altered by long-term atmospheric [CO2] enrichment under native or enhanced soil fertility. *Global Change Biol.* 24 (10), 4841–4856. <http://dx.doi.org/10.1111/gcb.14363>, URL <https://onlinelibrary.wiley.com/doi/10.1111/gcb.14363>.
- Wieser, G., Hammerle, A., Wohlfahrt, G., 2008. The water balance of grassland ecosystems in the Austrian alps. *Arct. Antarct. Alp. Res.* 40 (2), 439–445. [http://dx.doi.org/10.1657/1523-0430\(07-039\)\[WIESER\]2.0.CO;2](http://dx.doi.org/10.1657/1523-0430(07-039)[WIESER]2.0.CO;2), URL [https://www.tandfonline.com/doi/full/10.1657/1523-0430\(07-039\)\[WIESER\]2.0.CO;2](https://www.tandfonline.com/doi/full/10.1657/1523-0430(07-039)[WIESER]2.0.CO;2).
- Yang, Y., McVicar, T.R., Yang, D., Zhang, Y., Piao, S., Peng, S., Beck, H.E., 2021. Low and contrasting impacts of vegetation CO2 and fertilization on global terrestrial runoff over 1982–2010: accounting for aboveground and belowground vegetation–CO2 and fertilization effects. *Hydrol. Earth Syst. Sci.* 25 (6), 3411–3427. <http://dx.doi.org/10.5194/hess-25-3411-2021>, URL <https://hess.copernicus.org/articles/25/3411/2021/>.
- Yang, Y., Roderick, M.L., Zhang, S., McVicar, T.R., Donohue, R.J., 2019. Hydrologic implications of vegetation response to elevated CO2 in climate projections. *Nature Clim. Change* 9 (1), 44–48. <http://dx.doi.org/10.1038/s41558-018-0361-0>, URL <https://www.nature.com/articles/s41558-018-0361-0>.
- Zhang, Y., Zheng, H., Zhang, X., Leung, L.R., Liu, C., Zheng, C., Guo, Y., Chiew, F.H.S., Post, D., Kong, D., Beck, H.E., Li, C., Blöschl, G., 2023. Future global streamflow declines are probably more severe than previously estimated. *Nat. Water* 1 (3), 261–271. <http://dx.doi.org/10.1038/s44221-023-00030-7>, URL <https://www.nature.com/articles/s44221-023-00030-7>.